$\gamma M^{23}K$, $\gamma M^{232}K$, and $\gamma L^{77}K$ Single Substitutions in the TF_1-ATPase Lower ATPase Activity by Disrupting a Cluster of Hydrophobic Side Chains†

Sanjay Bandyopadhyay and William S. Allison*

Department of Chemistry and Biochemistry, University of California at San Diego, La Jolla, California 92093-0601

Received April 7, 2004; Revised Manuscript Received May 26, 2004

ABSTRACT: In crystal structures of the bovine F_1-ATPase (MF_1), the side chains of γMet^{23}, γMet^{232}, and γLeu^{77} interact in a cluster. Substitution of the corresponding residues in the $\alpha_3\beta_3\gamma$ subcomplex of TF_1 with lysine lowers the ATPase activity to 2.3, 11, and 15%, respectively, of that displayed by wild-type. In contrast, TF_1 subcomplexes containing the $\gamma M^{23}C$, $\gamma M^{232}C$, and $\gamma L^{77}C$ substitutions display 36, 36, and 130%, respectively, of the wild-type ATPase activity. The ATPase activity of the $\gamma M^{23}C/\gamma M^{232}C$ double mutant subcomplex is 36% that of the wild-type subcomplex before and after cross-linking the introduced cysteines, whereas the ATPase activity of the $\gamma M^{23}C/L^{77}C$ double mutant increased from 50 to 85% that of wild-type after cross-linking the introduced cysteines. Only $\beta-\beta$ cross-links formed when the $\alpha_3(\beta E^{395}C)_3\gamma M^{23}C$ double mutant was inactivated with $CuCl_2$. The overall results suggest that the attenuated ATPase of the mutant subcomplexes containing the $\gamma M^{23}K$, $\gamma L^{77}K$, and $\gamma M^{232}K$ substitutions is caused by disruption of the cluster of hydrophobic amino acid side chains and that the midregion of the coiled−coil comprised of the amino- and carboxyl-terminal α helices of the γ subunit does not undergo unwinding or major displacement from the side chain of γLeu^{77} during ATP-driven rotation of the γ subunit.

The F_1-ATPase is the peripheral component of the F_oF_1-ATP synthases that catalyze the condensation of ADP with P_i driven by ion electrochemical gradients in energy transducing membranes. When separated from the F_o component in soluble form, F_1 is an ATPase comprised of five gene products with $\alpha_3\beta_3\gamma\delta\epsilon$ stoichiometry. Isolated F_1-ATPases contain six nucleotide binding sites, three of which are catalytic sites. The other three binding sites, called noncatalytic sites, do not have a well-defined functional role (*1*). Crystal structures of MF_1[1] have shown that catalytic sites are predominantly in β subunits at α/β interfaces, whereas noncatalytic sites are mostly in α subunits at different α/β interfaces (*2*−*4*). In the original crystal structure, the three noncatalytic sites are homogeneously liganded with MgAMP−PNP, whereas catalytic sites are heterogeneously liganded. One designated β_{TP} contains MgAMP−PNP, another designated β_{DP} contains MgADP, and the third site designated β_E is empty (*2*).

In crystal structures of MF_1, the elongated α and β subunits alternate to form an $(\alpha\beta)_3$ hexamer, the central cavity of which is occupied by an asymmetric coiled−coil comprised of the N- and C-terminal α helices of the γ subunit. A globular domain consisting of residues 50−197 of the γ subunit protrudes from that part of the coiled−coil that is outside the central cavity of the $(\alpha\beta)_3$ hexamer (*3*, *4*).

Single molecule studies have shown that the immobilized $\alpha_3\beta_3\gamma$ subcomplex of the TF_1-ATPase is a rotary motor. During ATP hydrolysis, sequential firing of the three catalytic sites drives counterclockwise rotation of the coiled−coil of the γ subunit within the core of the $(\alpha\beta)_3$ hexamer in discrete 120° steps (*5*, *6*). From molecular dynamics simulations using coordinates from crystal structures of MF_1, Ma et al. (*7*) proposed that during energy-driven ATP synthesis, clockwise rotation of the γ subunit is accompanied by unwinding and rewinding of the coiled−coil during each 120° rotational step. The simulations also indicate that the globular part of the γ subunit protruding from the coiled−coil undergoes a rocking motion during each 120° rotational step.

Figure 1 illustrates that the side chains of γM^{23} in the N-terminal α helix, γM^{232} in the C-terminal α helix, and γL^{77} in the protrusion are arranged in a cluster in the crystal structure of MF_1 in which Glu^{199} in β_{DP} is derivatized with DCCD (*3*). The nearest distances between the side chains of these residues in the frozen native (*3*) and $(MgADP{\cdot}AlF_4^-)_2$ (*4*) crystal structures of MF_1 are also listed in Table 2. Position γ-23 is occupied by Met in all but two sequences listed in Swiss-Prot/ TrEMBL including TF_1. Gln occupies this position in *Mycobacterium tuberculosis* and *Mycobacterium leprae*. The equivalent of γ-77 in MF_1 (γ-85 in TF_1)[2] is occupied by Leu in all but one of the γ subunits listed. Met occupies the equivalent position in *Haemophilus influenzae*. The equivalent of γ-232 in MF_1 (γ-241 in TF_1) is occupied by Met in all species listed.

† This work was supported by NIGMS Grant GM 16974 from the National Institutes of Health.

* To whom correspondence should be addressed. Telephone: (858) 534-3057. Fax: (858) 822-0079. E-mail: wsa@checfs2.ucsd.edu.

[1] Abbreviations: MF_1, TF_1, and EF_1, the F_1-ATPases from bovine heart mitochondria, the thermophilic *Bacillus* PS3, and *Escherichia coli*, respectively; AMP-PNP, 5′-adenylyl β,γ-imidophosphate; LDAO, lauryl dimethylamine oxide.

[2] Unless stated otherwise, residue numbers of MF_1 are used throughout. In MF_1, βE^{395} is equivalent to βE^{391} of TF_1, βL^{391} is equivalent to βL^{385} in TF1, γL^{77} is equivalent to γL^{85} of TF_1, and γM^{232} is equivalent to γM^{241} in TF_1.

10.1021/bi0493012 CCC: $27.50
Published on Web 06/30/2004

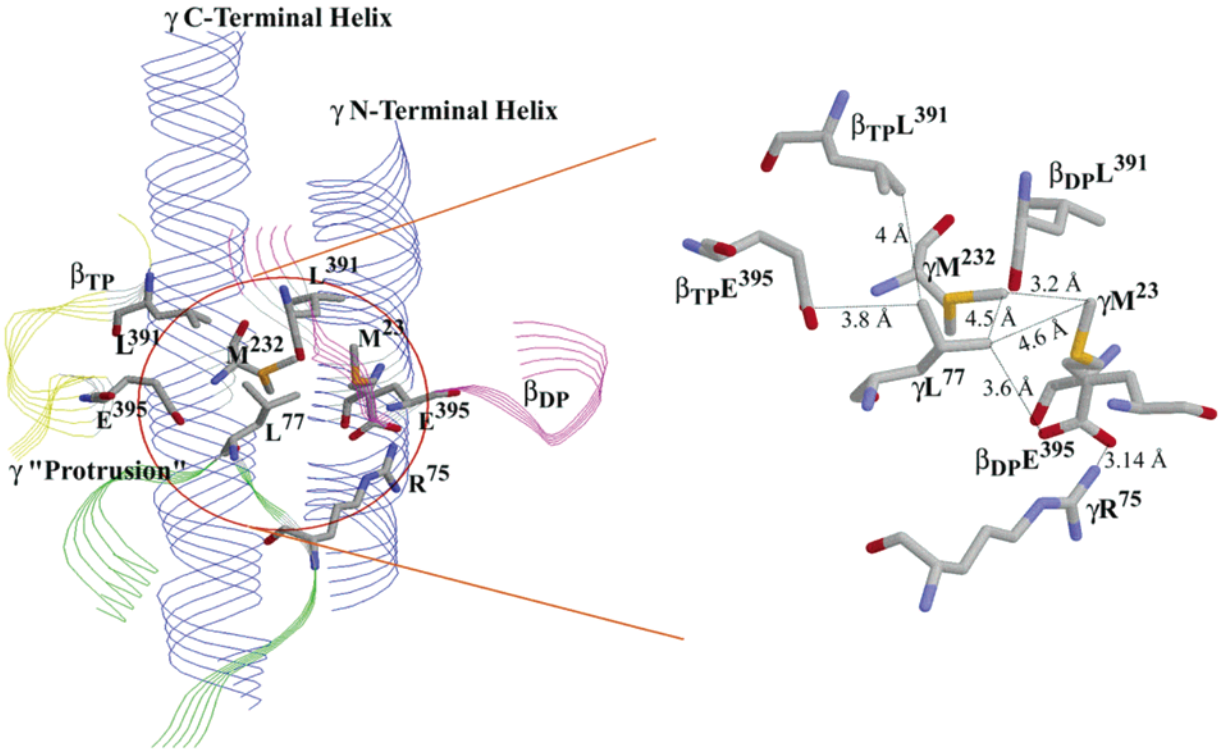

FIGURE 1: Relative positions of the side chains of γM^{23}, γL^{77}, γM^{232}, $\beta_{DP}L^{391}$, and $\beta_{TP}L^{391}$ in the crystal structure of MF_1 derivatized with DCCD: the figure was constructed from the coordinates of MF_1 obtained from Protein Data Bank entry 1E79 using the RasMol software program provided by Roger Sayle (Glaxo Wellcome Research and Development, Greenford, United Kingdom).

Table 1: Synthetic Oligonucleotides Used for Site-Directed Mutagenesis

mutation	oligonucleotide sequence[a]
$\gamma M^{23}C$[b]	5-CAAATTACAAAAGCGTGCGAAATGGTCTCG-3
$\gamma M^{241}C$[b]	5-GGATGACGGCGTGTAAGAACGCAACG-3
$\gamma L^{85}C$[b]	5-GGATCGCGGTTGTGCTGGCGCGTAC-3
$\gamma M^{23}K$[b]	5-CAAAAGCGAAGGAAATGGTCTCGAC-3
$\gamma M^{241}K$[b]	5-GATGACGGCGAAGAAGAACGCAAC-3
$\gamma L^{85}K$[b]	5-GGATCGCGGTAAAGCTGGCGCGTAC-3

[a] The bases changed are underlined. [b] These are TF_1 residue numbers. See footnote 1 for the corresponding residues in MF_1.

Table 2: Nearest Distances between Side Chains in the γ Subunit and the Side Chains of $\beta_{DP}L^{391}$ and $\beta_{TP}L^{391}$ in Crystal Structures of MF_1

residue pair	frozen native (Å)[a]	DCCD (Å)[b]	$(MgADP-AlF_4^-)_2$ (Å)[c]
$\gamma M^{23}-\gamma M^{232}$	3.80	3.32	3.16
$\gamma M^{23}-\gamma L^{77}$	3.80	4.27	5.41
$\gamma L^{77}-\gamma M^{232}$	4.17	4.55	3.38
$\beta_{DP}L^{391}-\beta_{TP}L^{391}$	5.04	4.13	4.77
$\gamma M^{23}-\beta_{DP}L^{391}$	4.67	3.56	4.02
$\gamma M^{23}-\beta_{TP}L^{391}$	7.69	7.42	7.26
$\gamma L^{77}-\beta_{DP}L^{391}$	5.54	4.77	4.00
$\gamma L^{77}-\beta_{TP}L^{391}$	3.70	4.06	4.17
$\gamma M^{232}-\beta_{DP}L^{391}$	5.10	4.85	4.76
$\gamma M^{232}-\beta_{TP}L^{391}$	5.36	5.69	4.66

[a] Obtained from Protein Data Bank entry 1E1Q. [b] Obtained from Protein Data Bank entry 1E79. [c] Obtained from Protein Data Bank entry 1H8E.

The rather strict homologies in these positions suggest that the cluster of interacting side chains might have a structure/function relationship. To determine if this is indeed the case, the catalytic characteristics of the $\alpha_3\beta_3\gamma$ subcomplexes containing the $\gamma M^{23}C$, $\gamma M^{232}C$, $\gamma L^{77}C$, $\gamma M^{23}K$, $\gamma M^{232}K$, and $\gamma L^{77}K$ single substitutions have been compared with those of the wild-type subcomplex. The catalytic characteristics of the $\alpha_3\beta_3(\gamma M^{23}C/M^{232}C)$ and $\alpha_3\beta_3(\gamma M^{23}C/L^{77}C)$ double mutant subcomplexes have also been compared before and after cross-linking the introduced cysteines to determine if cross-linking the N- and C-terminal α helices within the coiled−coil or between the coiled−coil and the protrusion affects catalysis.

In crystal structures of MF_1, the side chain of γMet^{23} is also within 5 Å of the side chain of $\beta_{DP}Glu^{395}$ (*3*). Al Shawi et al. (*8*) proposed that the severely attenuated ATPase activity displayed by the $\gamma M^{23}K$ mutant of the *Escherichia coli* F_1 might be caused by an ionized hydrogen bond between the introduced lysine side chain and the carboxylate of βGlu^{395}. Given that an earlier study showed that only $\beta-\beta$ cross-links formed upon treatment of the $\alpha_3(\beta E^{395}C)_3\gamma K^{36}C$ double-mutant subcomplex with $CuCl_2$ (*10*), the $\alpha_3(\beta E^{395}C)_3\gamma M^{23}C$ double-mutant subcomplex has also been prepared and characterized to determine if $\beta-\gamma$ cross-links form upon treatment of the double mutant with $CuCl_2$.

EXPERIMENTAL PROCEDURES

Generation and Expression of Plasmid Mutants. The expression plasmid pKK that encodes the α, β, and γ subunits of TF_1 was used for both site-directed mutagenesis and gene expression (*9*). Site-specific mutations in the expression plasmid were performed with PCR using the QuikChange site-directed mutagenesis kit from Stratagene. The wild-type and mutant plasmids were purified using the Wizard Plus miniprep kit from Promega. The primers (Invitrogen) and corresponding complements (not shown) that were used to incorporate the $\alpha_3\beta_3\gamma M^{23}C$, $\alpha_3\beta_3\gamma M^{232}C$,

$\alpha_3\beta_3\gamma L^{77}C$, $\alpha_3\beta_3\gamma M^{23}K$, $\alpha_3\beta_3\gamma M^{232}K$, and $\alpha_3\beta_3\gamma L^{77}K$ single substitutions in the wild-type pKK expression plasmid are listed in Table 1. The $\beta E^{395}C$ single mutant plasmid DNA (*10*) was used as template to generate the $\alpha_3(\beta E^{395}C)_3\gamma M^{23}C$ double mutant, and the $\alpha_3\beta_3\gamma M^{23}C/M^{232}C$ and $\alpha_3\beta_3\gamma M^{23}C/L^{77}C$ double mutants were generated using the $\gamma M^{23}C$ single mutant plasmid DNA as template. Introduction of each mutation was confirmed by DNA sequencing. The mutant plasmids were expressed in *E. coli* strain JM103 (*unc*$^-$). The wild-type and mutant $\alpha_3\beta_3\gamma$ subcomplexes were purified to homogeneity and stored as suspensions in 75% saturated ammonium sulfate at 4 °C as described by Matsui and Yoshida (*9*).

Analytical Methods. Endogenous nucleotides were removed from the wild-type and mutant subcomplexes before kinetic measurements and cross-linking by treatment with CDTA as described in detail previously (*10*). ATPase activity was determined spectrophotometrically in assay medium containing 2 mM ATP and 3 mM Mg^{2+} in 50 mM HEPES−KOH, pH 8.0 at 30 °C using an ATP regeneration system coupled to oxidation of NADH described previously (*10*). NADH oxidation was monitored at 340 nm with a Uvikon-XL double beam spectrophotometer. Traces were recorded within 3 s after initiating the reactions by injecting small volumes of enzyme solutions into 1 mL of assay medium. Protein concentrations were determined by the method of Bradford using Coomassie Blue from Pierce (*11*). SDS−polyacrylamide gel electrophoresis was performed on 12% Tris-Cl Ready Gels from Bio-Rad. After staining with 0.1% Coomassie Brilliant Blue R-250, gels were destained thoroughly and photographed.

Preparation of Reduced and Cross-Linked $\beta E^{395}C$ Single and $\beta E^{395}C/\gamma M^{23}C$, $\gamma M^{23}C/M^{232}C$, and $\gamma M^{23}C/L^{77}C$ Double-Mutant Subcomplexes. For complete reduction of the single or double-mutant subcomplexes, 1 mg/mL protein solutions in 50 mM Tris-Cl, pH 8.0 containing 0.1 mM EDTA were treated with 10 mM DTT for 2 h at 23 °C. To prepare the cross-linked $\alpha_3(\beta E^{395}C)_3\gamma$ single and $\alpha_3\beta_3\gamma M^{23}C/M^{232}C$, $\alpha_3\beta_3\gamma M^{23}C/L^{77}C$, or $\alpha_3(\beta E^{395}C)_3\gamma M^{23}C$ double-mutant subcomplexes, the completely reduced single and double mutant subcomplexes, at 1 mg/mL in 50 mM Tris-Cl, pH 8.0 were treated with either 100 or 500 μM $CuCl_2$ at 23 °C in the absence of DTT and EDTA. After complete oxidation of the single- or double-mutant subcomplexes as assessed by activity measurements or SDS−PAGE, excess $CuCl_2$ was removed from reaction mixtures by passing 100 μL aliquots of the oxidized protein samples through 1 mL centrifuge columns of Sephadex G-50 equilibrated with 50 mM Tris-Cl, pH 8.0 (*12*).

RESULTS

Comparison of Effects of NaN_3 and LDAO on the Hydrolysis of 2 mM ATP by the Wild-Type, $\gamma M^{23}C$, $\gamma M^{232}C$, $\gamma L^{77}C$, $\gamma M^{23}K$, $\gamma M^{232}K$, and $\gamma L^{77}K$ Single-Mutant Subcomplexes. Turnover-dependent entrapment of inhibitory MgADP occurs during hydrolysis of ATP by bovine heart MF_1, spinach CF_1, TF_1, and the wild-type $\alpha_3\beta_3\gamma$ subcomplex of TF_1 (*13*−*16*). In the case of the wild-type subcomplex, turnover-dependent inhibition is provoked by azide and is relieved by the nonionic detergent LDAO (*15*). Mutant subcomplexes have been characterized in which turnover-dependent entrapment of inhibitory MgADP is greater than that observed with wild-type (*16*−*18*), and others have been described in which entrapment of inhibitory MgADP is less than that observed with wild-type (*19*−*21*). Therefore, the ATPase activities of the mutant enzymes examined in this study have been assayed with and without azide or LDAO to determine if the amino acid substitutions alter propensity to entrap inhibitory MgADP in a catalytic site during turnover.

Figure 2 compares the effects of NaN_3 and LDAO on the rate of hydrolysis of 2 mM ATP catalyzed by the wild-type and single-mutant subcomplexes in the presence of an ATP regenerating system. In the absence of additions, the wild-type $\alpha_3\beta_3\gamma$ subcomplex hydrolyzes 2 mM ATP with a steady-state rate of 20 μmol of ATP hydrolyzed mg^{-1} min^{-1}. In the presence of 1 mM NaN_3, the rate of hydrolysis of 2 mM ATP by the wild-type subcomplex is inhibited nearly completely in a turnover-dependent manner. In the presence of 0.06% LDAO, the ATPase activity of wild-type subcomplex increases 4.3-fold.

In the absence of additions, the $\alpha_3\beta_3\gamma M^{23}C$ single-mutant subcomplex hydrolyzed 2 mM ATP at 36% of the rate exhibited by wild-type. In contrast, the $\alpha_3\beta_3\gamma M^{23}K$ single mutant hydrolyzed ATP at only 2.3% of the rate exhibited by wild-type. Both the $\gamma M^{23}C$ and $\gamma M^{23}K$ single mutant enzymes were more sensitive than wild-type to turnover-dependent inhibition induced by NaN_3 and were stimulated 8- and 11-fold, respectively, by LDAO. The catalytic characteristics of the $\gamma M^{232}C$ single-mutant subcomplex are similar to those of the $\gamma M^{23}C$ single mutant. The $\alpha_3\beta_3\gamma M^{232}C$ subcomplex hydrolyzed 2 mM ATP at 36% of the wild-type rate was nearly completely inhibited by 1 mM NaN_3 in a turnover-dependent manner and was stimulated 6-fold by 0.06% LDAO. The $\alpha_3\beta_3\gamma M^{232}K$ single-mutant subcomplex hydrolyzed 2 mM ATP at 11% of the wild-type rate as compared to 2.3% of the wild-type rate exhibited by the $\gamma M^{23}K$ single mutant. Hydrolysis of 2 mM ATP by the $\gamma M^{232}K$ single mutant enzyme was strongly inhibited by 1 mM NaN_3 and was accelerated 6-fold by LDAO. These results indicate that substitution of γMet^{23} and γMet^{232} with cysteine increases propensity to entrap inhibitory MgADP in a catalytic site during turnover about equally. Although both the $\gamma M^{23}K$ and the $\gamma M^{232}K$ mutant subcomplexes have greater propensity than the $\gamma M^{23}C$ and $\gamma M^{232}C$ mutants to entrap inhibitory MgADP in a catalytic site during turnover, the $\gamma M^{23}K$ mutant is more sensitive to MgADP inhibition.

In contrast, the $\gamma L^{77}C$ single mutant subcomplex hydrolyzes 2 mM ATP 30% faster than the wild-type subcomplex and is inhibited to a lesser extent than wild-type by azide. Furthermore, the rate of hydrolysis 2 mM ATP by the $\gamma L^{77}C$ single mutant was stimulated 2.6-fold by LDAO rather than 4.3-fold exhibited by the wild-type subcomplex. These characteristics suggest that the $\gamma L^{77}C$ substitution decreases the propensity to entrap inhibitory MgADP in a catalytic site during turnover. In contrast, the $\gamma L^{77}K$ single mutant subcomplex hydrolyzed 2 mM ATP at 15% of the wild-type rate and was inhibited to a greater extent than wild-type in the presence of azide indicating that it has greater propensity than wild-type to entrap inhibitory MgADP in a catalytic site during turnover. However, inconsistent with this premise, hydrolysis of 2 mM ATP by the $\gamma L^{77}K$ single mutant was stimulated only 1.6-fold by LDAO.

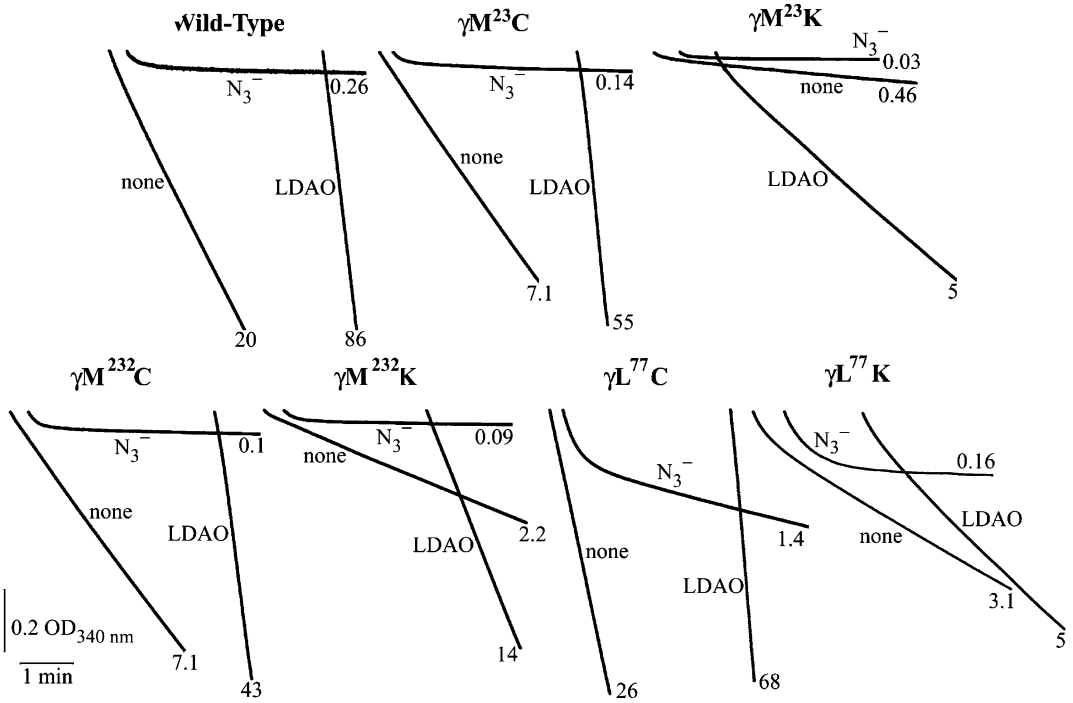

FIGURE 2: Comparison of the effects of NaN_3 and LDAO on hydrolysis of ATP by the wild-type and single mutant subcomplexes. Hydrolysis of 2 mM ATP was performed with an ATP regenerating system (*10*) in the presence of 3 mM $MgCl_2$ at 30 °C. Assays were initiated by injecting 2 μg of the wild-type or 5 μg each of the single mutants into 1 mL of assay medium in the presence or absence of 1 mM NaN_3 or 0.06% LDAO. The numbers on the traces represent the final rates of ATP hydrolysis recorded over the last 1 min of each assay are expressed in μmol of ATP hydrolyzed mg^{-1} min^{-1}.

Cross-Linking the Introduced Cysteines Does Not Affect the ATPase Activity of $\alpha_3\beta_3\gamma M^{23}C/M^{232}C$ Double-Mutant Subcomplex. Figure 3A illustrates that treatment of the $\alpha_3\beta_3\gamma M^{23}C/M^{232}C$ double-mutant subcomplex with 100 μM $CuCl_2$ for 2 h converts the γ subunit to a form that has increased electrophoretic mobility during SDS−PAGE, indicating cross-linking of the introduced cysteines. The extent of cross-linking was not affected by including stoichiometric or 0.2 mM MgADP during treatment with $CuCl_2$. Figure 3B shows that treatment of the reduced double mutant with $CuCl_2$ for 3 h did not significantly alter the characteristics of hydrolysis of 2 mM ATP in the presence or absence of NaN_3 or LDAO.

Treatment of $\alpha_3\beta_3\gamma M^{23}C/L^{77}C$ Double Mutant with $CuCl_2$ Activates ATPase Activity. Figure 4A shows that in the absence of added MgADP (open circles), treatment of the fully reduced $\alpha_3\beta_3\gamma M^{23}C/L^{77}C$ double-mutant subcomplex with 100 μM $CuCl_2$ in the absence of DTT slowly increases the rate of hydrolysis of 2 mM ATP. Under these conditions, acceleration of activity plateaus after 3−4 h when the specific activity is about 17 μmol of ATP hydrolyzed mg^{-1} min^{-1}. The rate of acceleration of ATPase activity was significantly increased when either stoichiometric (closed tilted squares) or 200 μM MgADP (closed circles) was added to the reduced enzyme before the addition of $CuCl_2$. When the fully reduced or the $CuCl_2$-treated double mutant was submitted to SDS−PAGE, the electrophoretic mobility of the γ subunit was the same as that observed with the wild-type subcomplex. Given that treatment with $CuCl_2$ activates the ATPase activity markedly, it appears that the loop formed upon formation of a disulfide bond between γCys^{23} and γCys^{77} in the double mutant does not alter mobility of the γ subunit during SDS−PAGE.

Figure 4B illustrates the kinetic characteristics of the $\gamma M^{23}C/L^{77}C$ double mutant before and after maximal activation with $CuCl_2$ in the absence of added MgADP. The reduced $\gamma M^{23}C/L^{77}C$ double mutant hydrolyzes 2 mM ATP with a specific activity of 10 μmol of ATP hydrolyzed mg^{-1} min^{-1}, which is 50% of the wild-type rate. The reduced mutant is less sensitive than wild-type to azide inhibition. It was stimulated to about the same extent as wild-type by LDAO. Compared to the wild-type subcomplex, the cross-linked $\gamma M^{23}C/L^{77}C$ double mutant is less sensitive to azide inhibition. It was stimulated only 1.7-fold by LDAO instead of 4.3-fold exhibited by the wild-type.

Only $\beta-\beta$ Cross-Links Form during Slow Inactivation of the $\alpha_3(\beta E^{395}C)_3(\gamma M^{23}C)$ Double Mutant with $CuCl_2$. Figure 5A shows that only $\beta-\beta$ cross-links formed when the $\alpha_3(\beta E^{395}C)_3(\gamma M^{23}C)$ double-mutant subcomplex was treated with 500 μM $CuCl_2$ for 24 h at room temperature in the presence or absence of stoichiometric or 200 μM MgADP. The same results were obtained in an earlier study when the $\alpha_3(\beta E^{395}C)_3\gamma$ single-mutant subcomplex was slowly inactivated with $CuCl_2$ under the same conditions (*10*). Figure 5B shows that the characteristics of hydrolysis of 2 mM ATP by the reduced $\alpha_3(\beta E^{395}C)_3(\gamma M^{23}C)$ double mutant are essentially the same as those obtained with the $\alpha_3(\beta E^{395}C)_3\gamma$ single mutant.

DISCUSSION

The catalytic characteristics of the $\gamma M^{23}C$ and $\gamma M^{232}C$ single mutants and those of the cross-linked and reduced forms of the $\gamma(M^{23}C/M^{232}C)$ double mutant are very similar. In the absence of additions, each mutant form hydrolyzes 2 mM ATP at about 35% of the wild-type rate. The mutant subcomplexes exhibit nearly identical patterns of turnover-

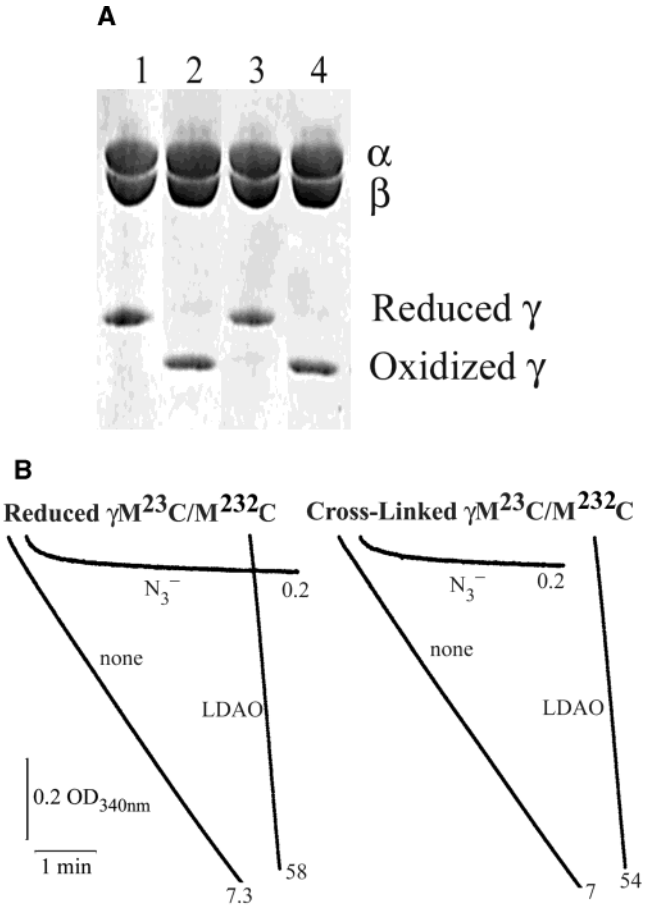

FIGURE 3: Cross-linking the introduced cysteines in the $\alpha_3\beta_3$-($\gamma M^{23}C/M^{232}C$) double mutant does not affect ATPase activity. (A) Following complete reduction of the double mutant subcomplex as described under Experimental Procedures, DTT and EDTA were removed by passing the enzyme solution through centrifuge columns of Sephadex G-50 that were equilibrated with 50 mM Tris-HCl, pH 8.0. The DTT-free, reduced enzyme at 1 mg/mL, was treated with 100 μM $CuCl_2$ in the presence and absence of 1 mM $MgCl_2$ and 0.2 mM ADP for 2 h, at which time excess $CuCl_2$, $MgCl_2$, and ADP were removed by passing 100 μL aliquots through 1 mL centrifuge columns of Sephadex G-50 that were equilibrated with 50 mM Tris-HCl, pH 8.0. Samples of 8 μg each were submitted to SDS−PAGE as described under Experimental Procedures. Lane 1: reduced enzyme plus 10 mM DTT; lane 2: reduced enzyme plus 100 μM $CuCl_2$; lane 3: reduced enzyme plus 1 mM $MgCl_2$ and 0.2 mM ADP; and lane 4, reduced enzyme plus 1 mM $MgCl_2$ and 0.2 mM ADP followed by 100 μM $CuCl_2$. (B) Comparison of hydrolysis of 2 mM ATP by the $\gamma M^{23}C/M^{232}C$ double mutant. Assays were initiated by injecting 5 μg of 1 mg/mL solutions of the reduced or oxidized double mutant subcomplex into 1 mL of assay medium containing 2 mM ATP plus 3 mM $MgCl_2$ in the presence and absence of 1 mM NaN_3 or 0.06% LDAO as specified. The numbers on the traces represent the final rates of ATP hydrolysis recorded over the last 1 min of each assay expressed in μmol of ATP hydrolyzed mg^{-1} min^{-1}.

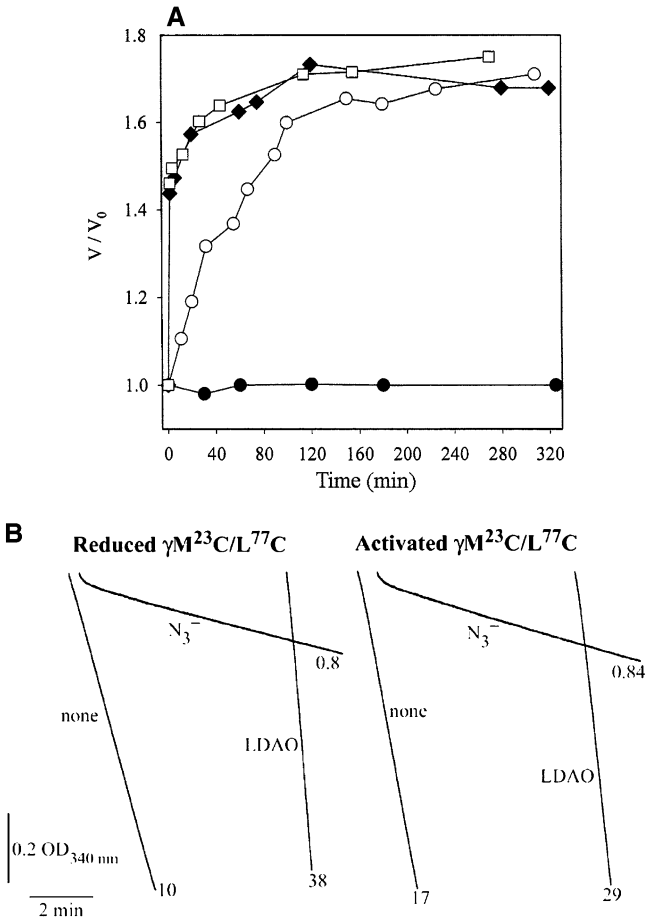

FIGURE 4: Treatment of the reduced $\alpha_3\beta_3\gamma(M^{23}C/L^{77}C)$ double mutant with $CuCl_2$ stimulates ATPase activity. The reduced double mutant subcomplex was freed of DTT and EDTA as described in the legend of Figure 3. (A) Time-dependent activation in the presence and absence of MgADP. Solutions of the reduced $M^{23}C/L^{77}C$double mutant at 1 mg/mL in 50 mM Tris-HCl, pH 8.0 were treated with 1 mM $MgCl_2$ and 0.2 mM ADP, closed circles; 100 μM $CuCl_2$, open circles; 1 mM $MgCl_2$ and 2.85 μM ADP followed by 100 μM $CuCl_2$, tilted closed squares; and 1 mM $MgCl_2$ and 0.2 mM ADP followed by 100 μM $CuCl_2$, open squares. (B) Comparison of the effects of LDAO and azide on ATPase activity before and after activation with 100 μM $CuCl_2$. Assays were initiated by injecting 5 μg of 1 mg/mL solutions of the reduced or oxidized double mutant subcomplex into 1 mL of assay medium containing 2 mM ATP plus 3 mM $MgCl_2$ in the presence and absence of 1 mM NaN_3 or 0.06% LDAO as specified. The numbers on the traces represent the final rates of ATP hydrolysis recorded over the last 1 min of each assay expressed in μmol of ATP hydrolyzed mg^{-1} min^{-1}.

dependent inhibition by NaN_3. Moreover, the ATPase activities of the four mutant forms are stimulated to about the same extent (6−8-fold) in the presence of LDAO. The finding that the catalytic characteristics of the $\gamma(M^{23}C/M^{232}C)$ double mutant are essentially the same before and after cross-linking the introduced cysteines indicates that the coiled−coil comprised of the N- and C-termini of the γ subunit does not unwind in the vicinity of these residues during rotation of the γ subunit driven by ATP hydrolysis. However, given that the γ subunit is connected to the ring of c subunits of F_o in the intact TF_oF_1-ATP synthase, it is possible that unwinding and rewinding of this region of the coiled−coil in the γ subunit might occur during ATP synthesis driven by proton translocation, the process simulated by Ma et al. (*7*). If this is indeed the case, the coiled−coil would also unwind and rewind during ATP-driven proton translocation catalyzed by the intact ATP synthase.

In contrast, the rate of hydrolysis of 2 mM ATP catalyzed by the $\gamma L^{77}C$ single-mutant subcomplex is 30% greater than that observed with the wild-type subcomplex. Furthermore, the rate of ATP hydrolysis by the reduced $\gamma(M^{23}C/L^{77}C)$ double mutant is 50% of the wild-type rate rather than 35% of the wild-type rate observed with the reduced $\gamma(M^{23}C/M^{232}C)$ double mutant. After cross-linking the introduced cysteines in the $\gamma(M^{23}C/L^{77}C)$ double mutant, the hydrolytic

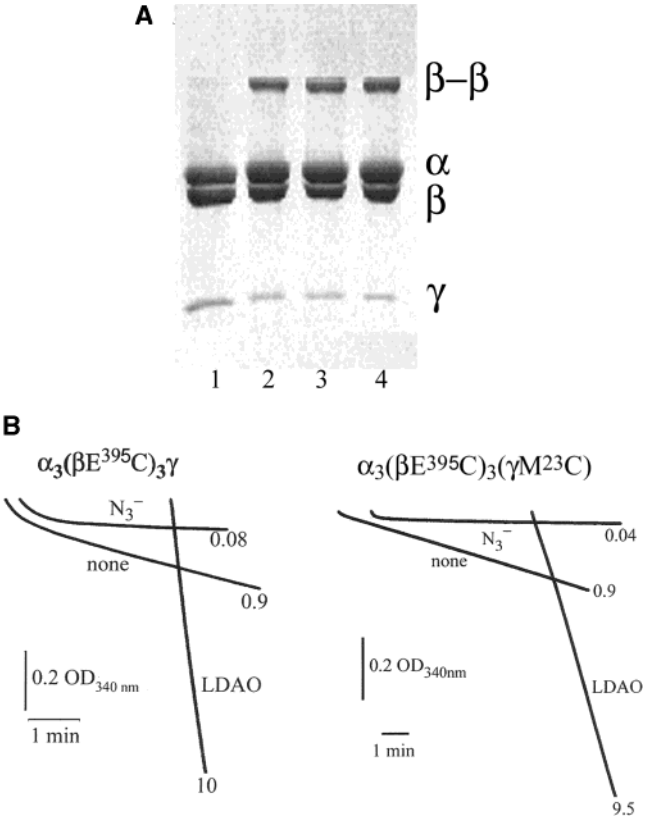

FIGURE 5: Only $\beta-\beta$ cross-links formed when the $\alpha_3(\beta E^{395}C)_3(\gamma M^{23}C)$ double mutant was treated with $CuCl_2$. (A) The cross-linked species was resolved by SDS−PAGE before and after oxidation of the $\alpha_3(\beta E^{395}C)_3(\gamma M^{23}C)$ double mutant subcomplex. The fully reduced, DTT-free double mutant prepared as described in the legend of Figure 3 was incubated at 1 mg/mL with either 10 mM DTT or 500 μM $CuCl_2$ in the presence or absence of MgADP for 24 h. Samples of 7 μg each were submitted to SDS−PAGE as described under Experimental Procedures. The samples submitted to electrophoresis contained the following: lane 1, enzyme plus 10 mM DTT; lane 2, enzyme plus 500 μM $CuCl_2$; lane 3, enzyme plus 1 mM $MgCl_2$ and 2.85 μM ADP followed by 500 μM $CuCl_2$; and lane 4, enzyme plus 1 mM $MgCl_2$ and 1 mM ADP followed by 500 μM $CuCl_2$. (B) Comparison of the effects of 1 mM NaN_3 and 0.06% LDAO on hydrolysis of 2 mM ATP by the reduced $\beta E^{395}C$ single and the $\alpha_3(\beta E^{395}C)_3(\gamma M^{23}C)$ double-mutant subcomplexes. The traces for the $\alpha_3(\beta E^{395}C)_3\gamma$ single mutant are taken from (*10*) and represent hydrolysis of 2 mM ATP by 10 μg of enzyme. The traces for the $\alpha_3(\beta E^{395}C)_3(\gamma M^{23}C)$ double mutant were obtained with 5 μg of enzyme. The numbers on the traces represent the final rates of ATP hydrolysis recorded over the last 1 min of each assay expressed in μmol of ATP hydrolyzed mg^{-1} min^{-1}.

rate increases to 85% of the wild-type rate indicating that the γ protrusion does not undergo significant displacement from the coiled−coil during ATP hydrolysis in the vicinity of γL^{77}.

The mutant forms containing the $\gamma L^{77}C$ substitution are also somewhat less sensitive to turnover-dependent inhibition by azide ion than wild type and the single and double mutants containing the $\gamma M^{23}C$ and $\gamma M^{232}C$ substitutions. This behavior suggests that the $\gamma L^{77}C$ substitution lowers the propensity for entrapment of inhibitory MgADP in a catalytic site during turnover. That the $\gamma L^{77}C$ mutant enzyme has greater ATPase activity and has less propensity than wild-type to entrap inhibitory MgADP in a catalytic site during turnover might be associated with dynamic interactions of the side chain γL^{77} with the side chains of Leu^{391} in β subunits during ATP-driven rotation of the γ subunit. In crystal structures of MF_1, the side chains $\beta_{DP}L^{391}$ and $\beta_{TP}L^{391}$ are within 5 Å of each other and are also near the side chains of γM^{23} and γL^{77} as shown in Table 2. These interactions are also illustrated in Figure 1.

Table 3: Nearest Distances between Side Chains in the γ Subunit and the Side Chains of $\beta_{DP}E^{395}$ and $\beta_{TP}E^{395}$ in Crystal Structures of MF_1

residue pair	frozen native (Å)[a]	DCCD (Å)[b]	$(MgADP-AlF_4^-)_2$ (Å)[c]
$\gamma M^{23}-\beta_{TP}E^{395}$	8.85	9.77	10.33
$\gamma M^{23}-\beta_{DP}E^{395}$	4.46	4.72	5.20
$\gamma L^{77}-\beta_{TP}E^{395}$	3.28	3.85	4.10
$\gamma L^{77}-\beta_{DP}E^{395}$	5.92	3.57	3.62
$\gamma M^{232}-\beta_{TP}E^{395}$	7.27	7.08	7.23
$\gamma M^{232}-\beta_{DP}E^{395}$	7.91	6.93	6.34
$\gamma M^{23}-\gamma R^{75}$		3.88	3.88
$\gamma R^{75}-\beta_{DP}{}^{395}$		3.16	3.87

[a] Obtained from Protein Data Bank entry 1E1Q. [b] Obtained from Protein Data Bank entry 1E79. [c] Obtained from Protein Data Bank entry 1H8E.

It is possible that the 30% greater ATPase activity of the $\gamma L^{77}C$ single mutant over that of wild-type reflects perturbation of dynamic interactions of the hydrophobic cluster in γ with the Leu^{391} side chains in β subunits during rotation of the γ subunit. During each 120° step of rotation of the γ subunit driven by sequential firing of catalytic sites during ATP hydrolysis, β subunits undergo $\beta_{DP} \rightarrow \beta_E$, $\beta_E \rightarrow \beta_{TP}$, and $\beta_{TP} \rightarrow \beta_{DP}$ interconversions. In the concerted interconversions, the side chain of $\beta_{TP}L^{391}$ loses contact with $\beta_{DP}L^{391}$ as β_E binds ATP and closes. This drives opening of β_{DP} that is accompanied by dissociation of products. In this process, the side chains of γM^{23} and γL^{77} must switch partners with the βL^{391} side chains as β subunits alternate between open and closed conformations. Substitution of γLeu^{77} with Cys might accelerate this process. The dynamic interactions between the side chains in the hydrophobic cluster in γ with the side chains of L^{391} in β subunits might be partly responsible for driving counterclockwise rotation of the γ subunit during ATP hydrolysis. The finding that the $\gamma M^{23}K$, $\gamma M^{232}K$, and $\gamma L^{77}K$ single mutants have considerably lower ATPase activity than the corresponding single mutants containing introduced cysteines is consistent with the argument that the side chains of γM^{23}, γM^{232}, and γL^{77} interact dynamically with the side chains of βL^{191} residues during ATP hydrolysis.

In crystal structures of MF_1 derivatized with DCCD and MF_1 containing MgADP-fluoroaluminate complexes bound to two catalytic sites, the guanidinium of γR^{75} is within 3.9 Å of the carboxylate of $\beta_{DP}E^{395}$ as shown in Table 3. In an earlier study, it was shown that $\beta-\gamma$ cross links formed rapidly when the $\beta E^{395}C/\gamma R^{75}C$ double-mutant subcomplex of TF_1 was treated with $CuCl_2$. This supports the prediction of Ma et al. (*7*), based on molecular dynamics simulations, that the side chain of γR^{75} is part of an ionic track comprised of positively charged side chains on the γ subunit and negatively charged residues in DELSEED segments of β subunits that guides rotation of the γ subunit during ATP synthesis. However, only $\beta-\beta$ cross-links formed when the $\beta E^{395}C/\gamma K^{36}C$ double-mutant subcomplex of TF_1 was slowly inactivated with $CuCl_2$ indicating that γK^{36} in TF_1 is not part of the ionic track proposed by Ma et al. (*7*).

The observation that only $\beta-\beta$ cross-links formed when the $\beta E^{395}C/\gamma M^{23}C$ mutant was treated with $CuCl_2$ suggests that the attenuated ATPase activity of the $\gamma M^{23}K$ single mutant is caused by disruption of hydrophobic interactions rather than introduction of electrostatic interactions between the introduced lysine and the carboxylates of E^{395} in β subunits. The latter alternative was proposed by Al Shawi et al. (*8*) to explain the low ATPase activity of the $\gamma M^{23}K$ mutant of the *E. coli* F_1-ATPase. That the ATPase activity of the $\gamma L^{77}K$ mutant is 15% of the wild-type rate, whereas the ATPase activity of the $\gamma M^{23}K$ mutant is 2.3% of the wild-type rate, supports the premise that disruption of the hydrophobic cluster is responsible for the attenuated ATPase activity accompanying the $\gamma M^{23}K$ substitution. The side chain of γL^{77} is significantly closer to the side chain of βE^{395} in crystal structures of MF_1 as shown in Table 3. If electrostatic interactions between the introduced lysines and the carboxylates of E^{395} in β subunits were responsible for the attenuated activities observed, it would expect that the $\gamma L^{77}K$ single mutant would have lower ATPase activity than the $\gamma M^{23}K$ single mutant. Clearly, this is not the case.

REFERENCES

1. Yoshida, M., Muneyuki, E., and Hisabori, T. (2001) ATP synthase—a marvelous rotary engine of the cell, *Nat. Rev./Mol. Cell Biol. 2*, 669−677.
2. Abrahams, J. P., Leslie, A. G. W., Lutter, R., and Walker, J. E. (1994) Structure at 2.8 Å resolution of F_1-ATPase from bovine heart mitochondria, *Nature 370*, 621−628.
3. Gibbons, C., Montgomery, M. G., Leslie, A. G. W., and Walker, J. E. (2000) The structure of the central stalk in bovine F_1-ATPase at 2.4 Å resolution, *Nat. Struct. Biol. 7*, 1055−1061.
4. Menz, R. I., Walker, J. E., and Leslie, A. G. W. (2001) Structure of bovine mitochondrial F_1-ATPase with nucleotide bound to all three catalytic sites: implications for mechanism of rotary catalysis, *Cell 106*, 331−341.
5. Noji, H., Yasuda, R., Yoshida, M., and Kinosita, K., Jr. (1997) Direct observation of the rotation of F_1-ATPase, *Nature 386*, 299−302.
6. Yasuda, R., Noji, H., Kinosita, K., Jr., and Yoshida, M. (1998) F_1-ATPase is a highly efficient molecular motor that rotates with discrete 120° steps, *Cell 93*, 1117−1124.
7. Ma, J., Flynn, T. C., Cui, Q., Leslie, A. G. W., Walker, J. E., and Karplus, M. (2002) A dynamic analysis of the rotation mechanism for conformational change in F(1)-ATPase, *Structure 10*, 921−931.
8. Al-Shawi, M. K., Ketchum, C. J., and Nakamoto, R. K. (1997) Energy coupling, turnover, and stability of the F_oF_1 ATP synthase are dependent on the energy of interaction between γ and β subunits, *J. Biol. Chem. 272*, 2300−2306.
9. Matsui, T., and Yoshida, M. (1995) Expression of wild-type and the Cys-/ Trp-less $\alpha_3\beta_3\gamma$ complex of thermophilic F_1-ATPase in *Eschericia coli*, *Biochim. Biophys. Acta 1231*, 139−146.
10. Bandyopadhyay, S., and Allison, W. S. (2004) The Ionic Track in the F_1-ATPase from the Thermophilic *Bacillus* PS3, *Biochemistry 43*, 2533−2540.
11. Bradford, M. M. (1976) A rapid and sensitive method for the quantitation of microgram quantities of protein utilizing the principle of protein−dye binding, *Anal. Biochem. 72*, 248−254.
12. Penefsky, H. S. (1977) Reversible binding of P_i by beef heart mitochondrial adenosine triphosphatase, *J. Biol. Chem. 252*, 2891−2899.
13. Jault, J.-M., and Allison, W. S. (1993) Slow Binding of ATP to Noncatalytic Nucleotide Binding Sites which Accelerates Catalysis Is Responsible for Apparent Negative Cooperativity Exhibited by the Bovine Mitochondrial F_1-ATPase, *J. Biol. Chem. 268*, 1558−1566.
14. Murataliev, M. B., and Boyer, P. D. (1992) The mechanism of stimulation of MgATPase activity of chloroplast F_1-ATPase by noncatalytic adenine-nucleotide binding, *Eur. J. Biochem. 209*, 681−687.
15. Paik, S. R., Jault, J.-M., and Allison, W. S. (1994). Inhibition and inactivation of the F_1 adenosinetriphosphatase from *Bacillus* PS3 by dequalinium and activation of the enzyme by lauryl dimethylamine oxide, *Biochemistry 33*, 126−132.
16. Jault, J.-M., Matsui, T., Jault, F. M., Kaibara, C., Muneyuki, E., Yoshida, M., Kagawa, Y., and Allison, W. S. (1996) The $\alpha_3\beta_3\gamma$ complex of the F_1-ATPase from Thermophilic *Bacillus* PS3 containing the $\alpha D^{261}N$ substitution fails to dissociate inhibitory MgADP from a catalytic site when ATP binds to noncatalytic sites, *Biochemistry 34*, 16412−16418.
17. Matsui, T., Muneyuki, E., Honda, M., Allison, W. S., Dou, C., and Yoshida, M. (1997) Catalytic activity of the $\alpha_3\beta_3\gamma$ complex of F_1-ATPase without noncatalytic nucleotide binding site, *J. Biol. Chem. 272*, 8215−8221.
18. Ren, H., and Allison, W. S. (2000) Substitution of βGlu^{201} in the $\alpha_3\beta_3\gamma$ subcomplex of the F_1-ATPase from the thermophilic *Bacillus* PS3 increases affinity of catalytic sites for nucleotides, *J. Biol. Chem. 275*, 10057−10062.
19. Bandyopadhyay, S., Valder, C. R., Huynh, H. G., Ren, H., and Allison, W. S. (2002) The $\beta G^{156}C$ substitution in the F_1-ATPase from the thermophilic *Bacillus* PS3 affects catalytic cooperativity by destabilizing the closed conformation of the catalytic site, *Biochemistry 41*, 14421−14429.
20. Dong, K., Ren, H., and Allison, W. S. (2002) The fluorescence spectrum of the introduced tryptophans in the $\alpha_3(\beta F^{155}W)_3\gamma$ subcomplex of the F_1-ATPase from the thermophilic *Bacillus* PS3 cannot be used to distinguish between the number of nucleoside di- and triphosphates bound to catalytic sites, *J. Biol. Chem. 277*, 9540−9547.
21. Ren, H., and Allison, W. S. (2000) On what makes the γ subunit spin during ATP Hydrolysis by F_1, *Biochim. Biophys Acta 1458*, 221−233.

BI0493012